

Void Scaling and Void Profiles in CDM Models

S. Arbabi-Bidgoli^{*} and V. Müller[†]

Astrophysikalisches Institut Potsdam, An der Sternwarte 16, 14482 Potsdam, Germany

Received

ABSTRACT

An analysis of voids using cosmological N -body simulations of cold dark matter (CDM) models is presented. It employs a robust statistics of voids, that was recently applied to discriminate between data from the Las Campanas Redshift Survey (LCRS) and different cosmological models. Here we extend the analysis to 3D and show that typical void sizes D in the simulated galaxy samples obey a linear scaling relation with the mean galaxy separation λ : $D = D_0 + \nu \times \lambda$. It has the same slope ν as in 2D, but with lower absolute void sizes. The scaling relation is able to discriminate between different cosmologies. For the best standard Λ CDM model, the slope of the scaling relation for voids in the dark matter halos is too steep as compared to the LCRS, with too small void sizes for well sampled data sets.

By considering a range of CDM simulations we further investigate the scaling relation for voids within the distribution of dark matter halos and other properties of underdense regions. The scaling relation of voids for dark matter halos with increasing mass thresholds is even steeper than that for samples of galaxy-mass halos where we sparse sample the data. This shows the stronger clustering of more massive halos. Further, we find a correlation of the void size to its central and environmental average density. We study the evolution of the void size distribution of dark matter halos at redshifts up to $z = 3$ measuring the sizes in comoving coordinates. While there is little sign of an evolution in samples of small DM halos with $v_{circ} \approx 90$ km/s, voids in halos with circular velocity over $v_{circ} = 200$ km/s are larger at redshift $z = 3$ due to the smaller halo number density. The flow of dark matter from the underdense to overdense regions in an early established network of large scale structure is also imprinted in the evolution of the density profiles with a relative density decrease in void centers by $\Delta(\rho/\bar{\rho}) \simeq 0.18$ per redshift unit between $z = 3$ and $z = 0$.

Key words: cosmology: dark matter – galaxies: formation – large scale structure of the universe.

1 INTRODUCTION

Voids in the large scale structure of the universe are the focus of the present paper. The building blocks of the large scale structure in the universe are superclusters, filaments of galaxies, and great walls. These structure elements are separated by regions where the density of visible matter is much less than the average density. Although several investigations of voids have been carried out (cp. Müller et al. 2000 and references therein), some key questions remain open. Voids were found in different sizes and properties, depending on the objects observed. The lower space density of

clusters and groups of galaxies leads to larger voids as compared to galaxy samples. Of particular interest is the question of the fraction of the total volume contained in voids. Obviously the answer depends not only on the completeness and quality of the data, but also on the definition used for voids. Several authors differ in the way that voids are identified. While in early papers (e.g. Einasto et al 1983 and Oort 1983) a qualitative description was used, later authors used spherical or spheroidal shaped regions which were fitted into the low density regions, e.g. Einasto et al. (1989), El-Ad & Piran (2000), Plionis & Basilakos (2001) and most recently Hoyle & Vogeley (2001a,b). Aikio and Mähönen (1998) proposed a different approach using points of maximal distance to their nearest neighboring galaxy. Voids detected with this algorithm are arbitrary shaped, nearly convex regions con-

^{*} Email: sarbabi@aip.de

[†] Email: vmueller@aip.de

taining no galaxies as they are formed from a collection of subvoids. This method yields voids which are very similar to the results of our algorithm described below. These methods have the advantage of covering almost the total volume of the sample with voids, so one can determine robustly the volume fraction that is contained in voids of different void sizes. Consequently the volume fraction of voids is a function of the void size rather than a pure number as discussed below.

Using cosmological N -body simulations we can explore some of the selection effects arising while investigating data with complicated survey geometries and object selections. In a simulation the structure that forms and evolves due to gravitational clustering is fully known and accessible. Therefore it is possible to study properties of voids such as size, abundance and density of dark matter and small galaxy halos in the voids and in the environment of the voids. A drawback of this approach is that the relation of the dark matter distribution to visible matter such as galaxies and clusters of galaxies is still under investigation. A careful study of the underdense regions in dark matter density fields and a comparison with observed voids will allow us to gain further insight. One challenging idea that can be realised in the simulations is to run the clock backwards and make predictions concerning the void properties in the past at higher redshifts. The effect of a possible evolution is one of our main areas of interest.

Most of our analysis is concentrated on the presently most popular set of the cosmological parameters, the Λ CDM model. This model includes a cosmological constant $\Omega_\Lambda = 0.7$ with a matter content $\Omega_m = 0.3$. The resulting universe is spatially flat, a preference of inflation theory. There are presently several observations which cover different aspects of modern cosmology and independently favor this model among other cold dark matter scenarios. In particular we cite the recent measurements of the light curves of distant supernovae (Goldhaber et al. 2001), measurement of the acoustic peaks in the spectrum of the anisotropies of the cosmic microwave background (Jaffe et al. 2001), and the evolution of the number density of galaxy clusters (Borgani et al. 2001).

We propose to undertake an additional test of the popular Λ CDM model, by comparing abundance and properties of the voids that occur in large N -body simulations of this model against existing observations. Recently in an analysis of the Las Campanas Redshift Survey (LCRS) a reliable method of determining the voids, together with a robust statistics in terms of median and quartile values of the size distribution, has been developed and applied to discriminate between different cosmological models (Müller et al. 2000). There we studied the area fraction of voids in an unambiguous way. Voids in the previous literature are often defined as empty or nearly empty regions exceeding a certain arbitrary chosen minimum size. To be independent of such a minimum size, we identify voids of all sizes and let them occupy the total volume of the survey or the sample under study. A cumulative size distribution shows which fraction of space is covered by voids up to a certain size. This cumulative size distribution has a very similar shape in different parts

of the LCRS despite differences in sampling and possibly cosmic variance. It represents the self similarity of the void distribution and allows the definition of median and quartile values of void sizes.

Previously (Müller et al. 2000) we showed that the median and quartile values of the cumulative void size distribution in well defined samples obey a linear scaling relation with the mean separation of galaxies in the studied sample. The slope of this relation is an important characteristic for the clustering properties of the observed large scale structure, and it proves to be able of discrimination between cosmological models. The analysis of the voids in the volume-limited subsamples of the LCRS and the comparison to the mock samples constructed from different CDM models independently favors a model with positive vacuum energy Λ CDM (and/or models with a break in the primordial power spectrum of density fluctuations, Kates et al. 1995).

Here we want to extend this analysis to 3 dimensions and make use of the full information contained in large N -body simulations. In prospect of the upcoming surveys of the large scale structure, testing the expectations of the models will be possible in the near future. One of our aims is to trace the evolution of underdense regions in the universe, and closely related, the evolution of the void size distribution using simulated galaxy halos. These were obtained in various N -body simulations of the Λ CDM and the OCDM model with various box sizes and resolutions. Therefore we are able to explore the scope between large simulation boxes and high spatial resolution. We study the connection of the void size distribution to the network of high and low density regions of the large scale matter distribution. Thereby we extend the previous analytic and numeric approach of van de Weygaert & van Kampen (1993). Also we investigate the growth of the size of the underdense regions as well as the evolution of their density profiles.

The present paper is organized as follows. In the next Section we describe the method we adopted, and in Section 3 we present further analysis of voids in the LCRS. Section 4 contains a description of the CDM models and the simulations we use for our analysis. Section 5 is devoted to the study of voids and underdensity regions at present time $z = 0$ according to N -body simulations. The evolution of voids is finally examined in Section 6 by investigating the cumulative void size distribution at different epochs and the change of the corresponding averaged density profiles of the voids. We close with a discussion and give some prospects for the future.

2 SEARCHING AND QUANTIFYING VOIDS

The algorithm used for the identification of voids is analogous to the one employed in our previous paper (Müller et al. 2000). It is an adapted version of the void search algorithm originally proposed by Kauffmann and Fairall (1991). The principle of the algorithm can be sketched as follows. A density field is realised on a high resolution grid where each galaxy occupies one grid cell. First the largest void is found and the volume it occupies is assigned to it, so that no other void can enter this region. It proceeds to the next largest

void and continues until there remains no more empty space for voids. Since the number of occupied cells usually represents a negligible part of the total number of cells, the total volume in voids occupies almost the total volume of the survey.

Each time the void finder identifies a void, it starts with placing the largest possible base void which is a cube of empty cells with maximal length to the grid of the density field. The next step of the search goes along the six 2-dimensional faces of the base voids. Accumulations of empty cells are attached to the faces of the cubic shaped base void. The condition for this is that the area covered by empty cells is larger than two third of the face area. Tests show that there is no significant dependence on this condition. This step is repeated taking each added extension as the parent face for the next extension as long as the area condition holds. The procedure of adding extensions starts with placing the largest square of empty cells on this area and attach rows of empty cells to each side of the square. Also the length of the row has to exceed two third of the length of the base square. In the next step again the attached row is taken as the parent for the next extension along its own edge. After the end of this procedure, the empty cells of the identified void are marked, so that subsequent voids will not enter or connect to the region assigned to this void.

In case of the two dimensional surveys such as the LCRS subsamples, the basis of the void search is a square laying in the plane of the data. Therefore the algorithm starts with the second step, i.e. only the part with the squares and the rows is applied here.

Physical motivation of this procedure comes from the fact that underdense regions in the universe tend to evolve into a nearly spherical shape with time (cp. e.g. van de Weygaert & van Kampen 1993). While overdensity regions decouple from the cosmic expansion and collapse to pancakes, filaments and clusters, the underdense regions grow faster than the background Hubble expansion. This has the effect that the initial geometry, which might be arbitrary, evolves to a more convex shape during later epochs. The above scheme takes this into account in two steps. At first, the void search starts from cubic base voids. Then it adds extensions in a way that approximately conserves convexity. The algorithm identifies neighboring voids separately if a galaxy between them stops the extensions. The voids are not connected by tunnel or finger like structures. A tunnel between two compact voids is added to the larger void. It may enter the smaller void region and subdivide it, but this extension will not enclose the smaller void. The algorithm will later find the empty parts of the second smaller void and identify them as separate void regions. Therefore the present approach recognizes large voids more robustly.

In density fields constructed from redshift surveys or N -body simulations small voids are much more abundant. Because data quality and sample completeness can affect each individual void, in particular its size, shape or even existence, we need to define statistical values, representing large, medium sized and small voids. In order to study the void size distribution with samples of different density, we often dilute the simulated samples, and the stochastic di-

lution mimics the effect of sparse sampling in the observations and affects the occurrence of voids. As it was shown by Sheth (1996) the process of random dilution is linked to higher order correlations of the large scale galaxy distribution, in particular in the application to counts in cells statistics. Large voids are less probable to be produced purely by random dilution or sparse sampling. We regard them as more prominent for the large scale structure geometry.

3 2D VOID ANALYSIS OF THE LCRS

Different from our recent approach in the analysis of the LCRS, we do not use the length of the base void as the characteristic size of the voids. Often the volume contained in the extensions is comparable to the base void. Therefore we take this into consideration and define the diameter D of a sphere as an effective void size, that has a volume equal to the total volume of the void, base volume plus extensions. In case of the 2D LCRS data the diameter of a circle is used. Further we calculate a cumulative void size distribution, which shows how much of the total volume of the sample is contained in voids up to a certain size. This cumulative distribution is a statistically robust description of the voids as was shown in Müller et al. (2000). As representatives for typical void sizes in the galaxy distribution we compute the median and quartile values of the area fraction of voids for all samples. In Müller et al. (2000) it was shown that these values obey a linear scaling relation $D = D_0 + \nu \times \lambda$. The mean galaxy separation λ varies due to different sampling fractions in the analysed data and due to different galaxy densities for changing magnitude ranges. We always select volume limited data sets by imposing absolute magnitude limits. The residuum size D_0 – the offset of the void size at formally zero galaxy separation $\lambda = 0$ – describes the deviation of the scaling relation from pure proportionality. The galaxy separation varies due to different galaxy densities for the absolute magnitude cuts in selecting volume limited data sets, and in different sampling fractions in the LCRS slices.

To test the robustness of the scaling relation in the LCRS found in Müller et al. (2000), here we add 3 more analyses to the original one:

(1) The effects of varying sampling fraction in the data. Each of the 6 LCRS slices consists of more than 50 observational fields with varying fractions of measured galaxy redshifts. To obtain homogeneous sampling fractions, in our previous paper we randomly diluted all fields to the sampling fraction of the field with the minimum sampling. Here we repeat this approach 10 times to evaluate the variance of the void size distribution. The result and the fitted scaling relations are shown in Fig. 1 and in Table 1. The accuracy of the fits and the narrowness of the error ranges are remarkable. The different LCRS slices sample the voids in different parts of the universe homogeneously and lead to stable results. This is the basis for our cosmological conclusions.

(2) The effects of the grid orientation.

In addition to the original paper we treated systematic errors introduced by the grid orientation in the determination of the median and quartile sizes D . These were estimated

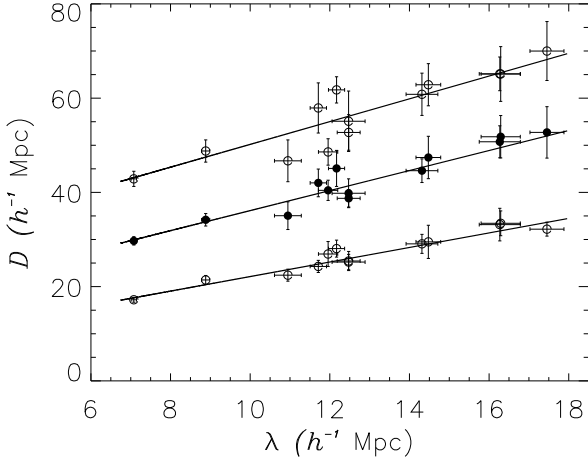


Figure 1. Median (filled circles), upper and lower quartile values (open circles) of void sizes in the LCRS volume limited samples. The error bars show the variation of the results obtained by repeating the selection of the subsamples.

by repeating the void search algorithm while the volume-limited LCRS samples were rotated with respect to the grid in steps of 10° . In Fig. 2 we show the scatter in median and quartile values due to the grid orientation by the vertical error bars on the diamonds and squares of the 14 volume limited data sets of the LCRS. Note that these data lie on a narrow range around the fits to the scaling relations shown by solid lines.

(3) The effect of further random dilution in homogeneous data sets.

We also studied the scaling relation for subsamples that stem from well sampled homogeneous datasets with mean galaxy separation $\lambda < 12h^{-1}\text{Mpc}$, that were further randomly diluted. Fig. 2 shows that the median and quartile void sizes of these data obey the same scaling relation (dashed lines) as in the originally studied data sets. The scatter is somewhat higher than the original data, which is due to the strong dilution of the galaxy numbers in the restricted volumes, especially concerning the median and the upper quartile. We take this as an upper bound on the variance of the void size distribution. These data underline that the scaling relation results from different galaxy densities in different samples and not from different galaxy properties as magnitude limits or galaxy types. The last point was discussed in detail in Müller et al. (2000).

The parameters of the scaling relations for the effective void sizes D are given in Table 1 first for the LCRS data using the different random selections described in point (1) above to estimate the error bars. The next row in the Table contains the parameters of the scaling relation using different grid orientations. The third row gives the results of a linear fit to the data including the diluted subsamples shown in Fig. 2. The three parameter sets agree remarkably well within the errors. However the scatter among the last sets of data is much larger and a χ^2 test of the fits implies

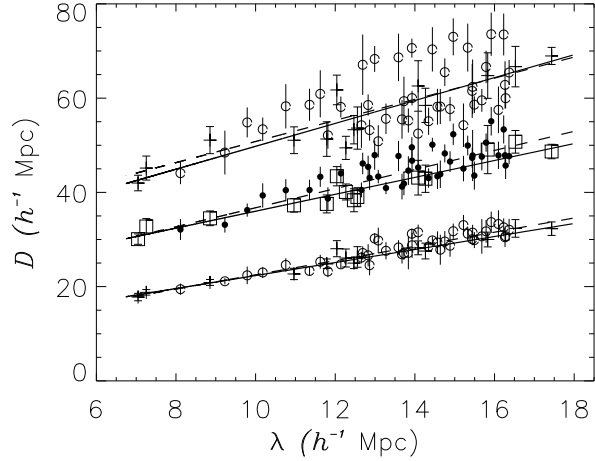


Figure 2. Median (large squares), upper and lower quartile values (diamonds) of void sizes in the LCRS volume limited samples with rotated grid of the density field. The scaling relation for these data sets are shown as solid lines. The quartile values for diluted subsamples of rich data sets ($\lambda < 12h^{-1}\text{Mpc}$) are given as open and filled circles with the scaling relations as dashed lines.

that only the errors contained in the first two lines can be regarded as reliable. For a comparison with our earlier paper, we also give the parameters for the scaling relation of the base void lengths. The absolute values are smaller because the base void lengths are smaller than the effective void sizes by about $\sqrt{2}$. The new analysis better takes into account the space covered by the extensions to the base void, as described above in Section 2.

4 CDM SIMULATIONS

To evaluate the void size distribution we performed a set of numerical simulations of realistic CDM cosmologies. As already shown previously (Müller et al. 2000), the void size distribution and the scaling relation depend on the cosmological parameters, and in particular on the power of the primordial fluctuation spectrum on large scales as described by the shape parameter $\Gamma = h\Omega_m$, where h is the dimensionless Hubble parameter $h = H_0/100 \text{ km/s/Mpc}$ and Ω_m the dimensionless matter density. Results that best reproduce the observed void size distribution were obtained for a standard ΛCDM model and for a model with a steplike primordial power spectrum, i.e. with a similar spectral shape as the widely discussed τCDM model. But even there it remained a significant discrepancy in the abundance of large voids and in the scaling relation of the void size distribution with the mean galaxy separation that becomes significant for the well sampled LCRS data sets. There we could not answer the question, whether a scale dependent bias can influence the void statistics, and in particular, what is the effect of the suppression of the galaxy formation probability in underdense regions. Such a suppression is sometimes denoted as large-scale bias (Doroshkevich et al. 1999). Furthermore,

Table 1. Void size scaling relation $D = D_0 + \nu \times \lambda$ for the quartiles in the LCRS, Λ CDM2 halos, Λ CDM1 mock, and OCDM mock samples, and Poisson samples.

samples	lower quartile	median	upper quartile
LCRS data samplings	$6.7 \pm 1.1 + (1.5 \pm 0.1) \times \lambda$	$14.9 \pm 2.0 + (2.1 \pm 0.2) \times \lambda$	$26.0 \pm 3.0 + (2.4 \pm 0.3) \times \lambda$
LCRS data for rotated grid	$8.5 \pm 1.0 + (1.4 \pm 0.1) \times \lambda$	$18.1 \pm 1.7 + (1.8 \pm 0.1) \times \lambda$	$25.5 \pm 2.5 + (2.4 \pm 0.2) \times \lambda$
LCRS data for diluted samples	$7.4 \pm 0.7 + (1.5 \pm 0.1) \times \lambda$	$16.5 \pm 1.3 + (2.0 \pm 0.1) \times \lambda$	$28.4 \pm 1.9 + (2.2 \pm 0.1) \times \lambda$
Base void sizes (Müller et al.)	$5.7 \pm 1.6 + (0.9 \pm 0.1) \times \lambda$	$11.8 \pm 2.9 + (1.1 \pm 0.2) \times \lambda$	$16.8 \pm 2.9 + (1.5 \pm 0.2) \times \lambda$
Λ CDM2 FOF-halos	$7.5 \pm 1.4 + (1.5 \pm 0.1) \times \lambda$	$9.6 \pm 1.2 + (2.0 \pm 0.1) \times \lambda$	$20.4 \pm 2.0 + (3.0 \pm 0.1) \times \lambda$
Λ CDM1 mocks	$2.0 \pm 0.9 + (1.8 \pm 0.1) \times \lambda$	$6.8 \pm 2.2 + (2.9 \pm 0.2) \times \lambda$	$19.7 \pm 1.9 + (2.9 \pm 0.2) \times \lambda$
OCDM mocks	$4.3 \pm 0.6 + (1.7 \pm 0.1) \times \lambda$	$11.2 \pm 0.9 + (2.3 \pm 0.1) \times \lambda$	$16.3 \pm 1.5 + (3.2 \pm 0.1) \times \lambda$
Poisson	$1.0 \pm 0.6 + (1.9 \pm 0.1) \times \lambda$	$0.0 \pm 0.9 + (3.0 \pm 0.1) \times \lambda$	$1.1 \pm 1.0 + (3.8 \pm 0.1) \times \lambda$

we could not answer the question for the relation of the void statistics in the narrow LCRS slices to the void statistics in full 3D galaxy samples. Both questions are addressed in the present paper using a set of realistic simulations with different procedures for galaxy identification in high resolution dark-matter simulations with different resolutions and box sizes.

Here we are not basically interested in discriminating between different cosmological models, therefore we restricted us mainly to the standard Λ CDM model with a density parameter $\Omega_m = 0.3$ and a Hubble constant $h = 0.7$, and we took as a comparison model only an open model OCDM with $\Omega_m = 0.5$ and $h = 0.6$. These parameters correspond to the models discussed in our earlier paper, and therefore, they are well suited to answer the mentioned questions. In Table 2 we give the simulation details, in particular the normalization by the linear mass variance on a $8 h^{-1}$ Mpc scale, σ_8 , the box size, and the mass and spatial resolution.

We perform two low resolution particle-mesh (PM) simulations with 256^3 particles in large boxes of $(500h^{-1}\text{Mpc})^3$ size using 512^3 grid cells, they are denoted as Λ CDM1 and OCDM. These simulations are similar to them used previously by (Doroshkevich et al. 1999) and Müller et al. (2000). With the large volume, they are well suited for discussing the relation of voids in the effective 2D slices of the LCRS to the true 3D void statistics. In these models we identified galaxies with single particles employing a nonlinear bias prescription detailed in Müller et al. (2000). In short, it employs the local density constructed from the neighboring particles and uses a threshold bias prescription for suppressing galaxy formation in low density regions, and a non-linear bias for particles in high density regions to model the merging and higher dark matter to galaxy ratio in high density regions as caused by the continuous merging in the hierarchical clustering process, cp. Cole et al. (1998).

Further we employ medium resolution particle-particle particle-mesh (P3M) simulations with the adaptive mesh refinement code of Couchmann (1991) using also 256^3 particles. These simulations, denoted Λ CDM1 and Λ CDM2, use boxes of $(280h^{-1}\text{Mpc})^3$ and $(200h^{-1}\text{Mpc})^3$, respectively, to test for the mass resolution dependence and the influence of the upper box size on the void statistics. The mass resolutions are 10^{11} and $4 \times 10^{10} h^{-1}M_\odot$, respectively, and we employ a spatial resolution of $50h^{-1}\text{kpc}$ and $40h^{-1}\text{kpc}$ in co-moving coordinates, cp. Table 2. This means we are able to resolve galaxy sized halos with 10 - 30 particles, but we also

get larger group and cluster sized halos that enclose systems of galaxy halos being overmerged in the medium resolution simulations. For the question of voids, the distribution of galaxies within groups and clusters is of minor importance. Therefore, we can identify field galaxy halos with systems of about 10 particles and we study the void distributions within these systems.

For the higher resolution simulation Λ CDM2 and Λ CDM3, we use a standard FOF halo finder, with a dimensionless linking length (in units of the mean particles separation) $b = 0.12$ (Λ CDM2) and $b = 0.17$ (Λ CDM3). The relatively small linking lengths effectively collect galaxy like halos also in high density regions of the simulation as in groups and clusters which is essential to get a realistic indication of void boundaries in higher density regions of the cosmic web. We impose a mass boundary of 13 DM-particles for Λ CDM2 and 8 dark matter particles for Λ CDM3, but for many analyses we further restrict the minimum of dark matter particles per halo. After identifying the halos for Λ CDM2, we check the virial theorem of the FOF-groups, and we split off groups with high kinetic energy T as compared to the potential energy $|W|$, $T > |W|$, to separate interacting or merging groups. To this aim we employ a 6D-group finder with a linking measure $\Delta r^2/r^2 + \Delta v^2/\sigma_v^2$ where r and σ_v are the effective (half-mass) radius and the velocity dispersion of the unbound groups. This concerns about 10% of the halos, with many halos having only a small number of DM particles. The splitting off of unbound halos adds about 2% to the equilibrium halos due to a fixed mass boundary for the final halos. Thereby we get about 53000 halos resampling possible galaxies in Λ CDM2 corresponding to a mean separation of $\lambda = 7.45h^{-1}\text{Mpc}$.

For Λ CDM3, we select halos at redshifts $z = 0, 1, 2, 3$ to check for the evolution of the void sizes. We take all halos selected with a linking length $b = 0.17$, finding about 160 000 objects with a mass limit of 8 dark matter particles, i.e. with a mean interparticle separation of $\lambda = 3.7h^{-1}\text{Mpc}$. At $z = 3$ this grows to $\lambda = 4.4h^{-1}\text{Mpc}$ due to the smaller number of halos at this redshift. We also employ a minimal circular velocity $v_{\text{circ}} > 200$ km/s for identifying normal mass galaxy halos which leads to about 23000 objects with a mean separation of $\lambda = 7h^{-1}\text{Mpc}$ at $z = 0$. The mean separation between halos grows at higher redshift, corresponding to $\lambda = 7.8h^{-1}\text{Mpc}$ at $z = 1$, $\lambda = 9.4h^{-1}\text{Mpc}$ at $z = 2$, and $\lambda = 13h^{-1}\text{Mpc}$ at $z = 3$ due to the mass increase in single halos by merger precesses and continuous mass accretion.

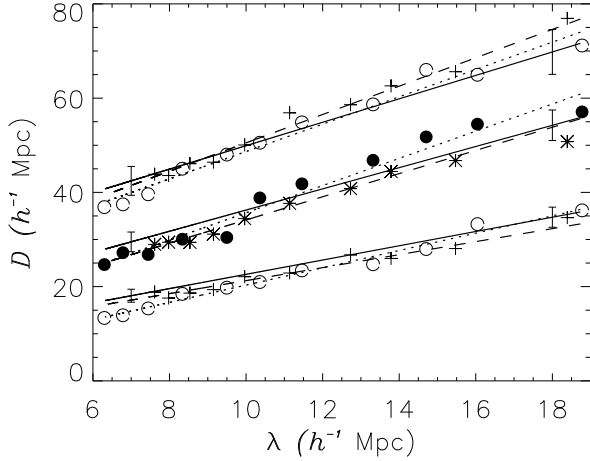


Figure 3. Scaling relation for median and quartile values of the void sizes of mock galaxy samples of the Λ CDM simulation in a $500h^{-1}\text{Mpc}$ box (filled and open circles and dotted lines) and halos in the Λ CDM2 simulation using a $280h^{-1}\text{Mpc}$ box (stars, crosses, and dashed lines), both in a geometry similar to the volume-limited sub-samples of LCRS (solid lines with error bars).

As shown in Müller et al. (2000) for the nonlinear biased mock catalogues, the halos reproduce well the two-point correlation function of galaxies in the LCRS in the redshift space (Tucker et al. 1997). Therefore they are reasonable test objects for the void statistics in the underlying CDM models.

The key questions of the simulations is whether they can reproduce the void size distribution, and in particular, the slope of the scaling relation for randomly diluted model galaxy samples. This characteristic measures the clustering properties in different parts of the universe observed by the LCRS. As it was shown in the previous paper, this slope is smaller for the LCRS samples than for the mock samples of N-body simulations, i.e. the median and upper quartile void sizes determined in the dense parts of the LCRS are larger. This was shown using mock samples having the same geometry as the LCRS samples. Especially in the well sampled parts the mock samples are not able to reproduce large voids. We complement this analysis by studying friend-of-friend dark matter halos of the Λ CDM2 simulation (cp. Table 2). In Fig. 3 we show that the scaling relation of voids in the Λ CDM mock samples (dotted lines) has almost the same steep slope as the scaling relation of halos in the Λ CDM2 simulation (dashed line, cp. also Table 1). In particular, it is significantly steeper than that from the LCRS (solid lines). The analysis of the halo samples was performed by constructing mock samples in a slice geometry as in the LCRS data, and we did a 2D void search as described in the last section. To resume, we cannot reproduce the typical voids in well sampled parts of the LCRS as shown on the left of Fig. 3.

The values found for the slopes of the scaling relations for the quartile and median values are given in Table 1. It

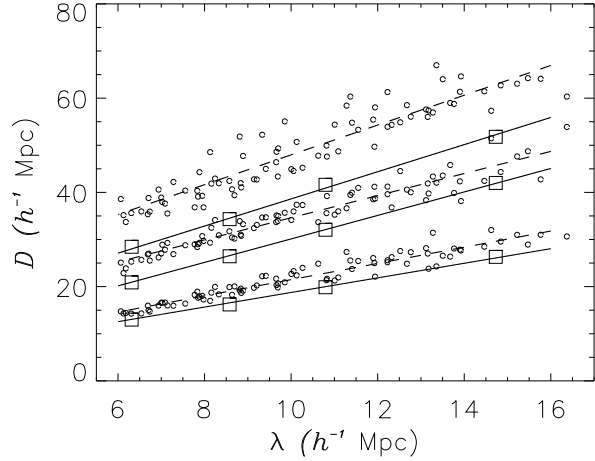


Figure 4. Comparison of the scaling relation in 2D and 3D for mock galaxy samples of the Λ CDM simulation in a $500h^{-1}\text{Mpc}$ box. The 2D results are based on a geometry similar to LCRS volume-limited samples (small circles and dashed lines). The 3D analysis leads to smaller values of the medium and quartile void sizes (large squares and solid lines), but the slope of the scaling relation is similar.

shows that the Λ CDM and Λ CDM1 mock samples and the Λ CDM2 FOF halos, that were constructed in different simulations, have similar scaling relations, in particular similar slopes. In all samples, we notice a statistically significant discrepancy to the LCRS.

5 VOIDS IN 3D AT REDSHIFT ZERO

While in Section 2 mock and halo samples with a slice geometry similar to the LCRS were analyzed, now we proceed to 3-dimensional samples obtained from simulations. As a typical example results from the Λ CDM simulation in a $500h^{-1}\text{Mpc}$ box are shown in Fig. 4. In 10 different cuts through the box, diluted mock samples with LCRS geometry were constructed. Their scaling with the mean separation is indicated by the dashed lines. Additionally the 3-dimensional algorithm is applied to the complete box. The full sample was also diluted in this case to investigate the behavior with lower sample density. Not only do the voids obey the scaling relation, but also the scatter is typically much lower. The scaling relations show the same slope, while there is an overall offset in the size. We regard this difference as a feature of the two dimensional slices. By observing only thin sheets in the underlying 3-dimensional galaxy sample, as it is the case with the LCRS slices, the effective size of voids *increases* due to missing galaxies in the bounded region of the slices. The increase in the absolute value of the scaling relation obviously depends on the mean depth of the slice in comparison to the mean void parameters, and we cannot connect it with any fundamental property of the galaxy distribution. The observed void sizes become on average 20 - 30% smaller in 3D, but the slope of the scaling relation of

Table 2. Cosmological N -body simulations

model	Ω_m	h	σ_8	box size	mass resolution	spatial resolution
Λ CDM1	0.3	0.7	0.87	$500h^{-1}\text{Mpc}$	$6 \times 10^{11} h^{-1}M_\odot$	$1.0 h^{-1}\text{Mpc}$
Λ CDM2	0.3	0.7	0.91	$280h^{-1}\text{Mpc}$	$10^{11} h^{-1}M_\odot$	$0.05 h^{-1}\text{Mpc}$
Λ CDM3	0.3	0.7	0.87	$200h^{-1}\text{Mpc}$	$4 \times 10^{10} h^{-1}M_\odot$	$0.04 h^{-1}\text{Mpc}$
OCDM	0.5	0.6	0.80	$500h^{-1}\text{Mpc}$	$10^{12} h^{-1}M_\odot$	$1.0 h^{-1}\text{Mpc}$

void sizes with the mean galaxy separation remains constant and represents an important characteristics of the hierarchy of the galaxy distribution in the cosmic web.

An important question to be addressed while studying void sizes is the dependence on the mass of the objects which represent the structure under analysis. From elementary considerations typical voids expected within the distribution of dwarf galaxies as an example must be different in size from the voids present in the large scale structure built by galaxy clusters, as an extreme opposite example. This is firstly due to the different number densities of these objects, and secondly because smaller objects are distributed more smoothly on average than large objects. Both of these properties affect the sizes of the voids, and they can be quantified by the scaling relation.

In Müller et al. (2000) we studied a possible dependence of median void sizes on the absolute magnitude. The magnitude range of galaxies in the LCRS varied between -20 and -21. This is a small range and as such we could not find any significant change in the sizes of voids. Here we study the dependence of void sizes on the FOF halo mass. Fig. 5 shows that the cumulative void size distribution bends towards larger void sizes with growing mass of the halos. A Λ CDM simulation in a $280h^{-1}\text{Mpc}$ box with a mass resolution of $10^{11}M_\odot$ was used. The lower cutoff in the mass range was set to $1.3 \times 10^{12}M_\odot$ for the most complete sample and to $1.5 \times 10^{13}M_\odot$ for the one with the lowest space density of halos. In the first case the sample contains all objects with a mass comparable to a milky way galaxy and higher. In the latter case the objects that remain in the sample are comparable to small galaxy groups. Because the number density of the identified halos decreases with growing mass, the structure of the samples is dominated by halos with masses near the lower end. Within the mass range of halos under investigation the median value of the void sizes increases from $25h^{-1}\text{Mpc}$ to twice this value. Obviously the void size distribution looks remarkably similar, cp. also Müller et al. (2000).

As a comparison of the scaling relation from sparse sampling and increasing mass, we construct randomly diluted samples with average mean separations λ similar to the halo samples with different masses. The diluted sets contain a mixture of high and low mass halos. Because of the higher abundance of the low mass halos, they dominate the diluted samples. Although dilution increases the void sizes, the voids in the diluted mixed samples are significantly smaller. As it is shown in Fig. 6 the difference grows to 20% for the sample with the largest halo masses. This effect is expected and easily explained by the picture of gravitational instability. Larger mass halos are more clustered according to

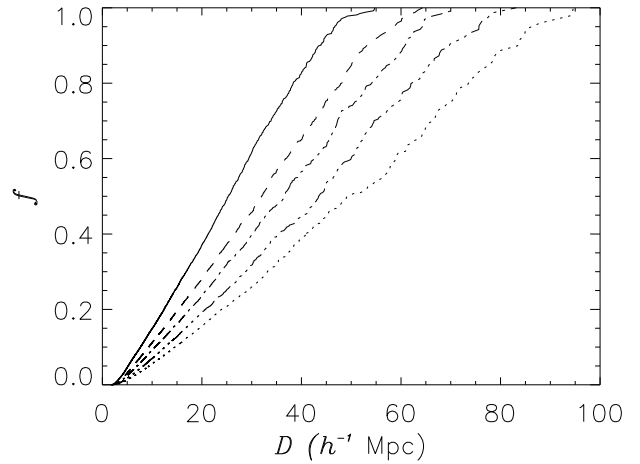


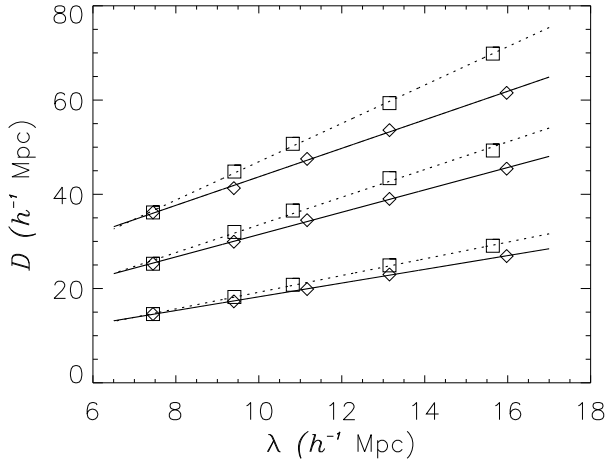
Figure 5. The cumulative void size distributions in the Λ CDM2 simulation in a $280h^{-1}\text{Mpc}$ box. We show the size distributions for dark matter halos with masses increasing from left to right, from $1.3 \times 10^{12} h^{-1}M_\odot$ (solid line), $3.2 \times 10^{12} h^{-1}M_\odot$ (dashed line), $6.0 \times 10^{12} h^{-1}M_\odot$ (dashed dotted line), $9.0 \times 10^{12} h^{-1}M_\odot$ (dashed three-dotted line) to $1.5 \times 10^{13} h^{-1}M_\odot$ (dotted line).

the higher amplitude of the 2-point correlation function of galaxy groups as compared to galaxies. Large and massive halos reside in the nodes of the large scale structure network, while the less massive ones are still streaming along pancakes and filaments towards these nodes. Their distribution is more homogeneous and less clustered. Table 3 compares the parameters of the scaling relation for these two differently selected series of halo samples. A similar change of the void size was found in Little & Weinberg (1994), but they did not derive the scaling relation of the void sizes under random dilution studied here. There were found larger voids if a biasing prescription for galaxy formation was applied. With the present approach we quantify this relation of object masses and void sizes.

An additional study illustrates the relation of the void sizes to their environmental and central density. For this purpose a smoothed density field was constructed in the dark matter distribution of the Λ CDM3 simulation in a $200h^{-1}\text{Mpc}$ box. In the first step the dark matter particles were distributed onto a grid with $0.5 h^{-1}\text{Mpc}$ per cell, using the cloud-in-cell method. After smoothing the density field with a Gaussian function ($\sigma = 1 h^{-1}\text{Mpc}$) a threshold overdensity of $\delta_{th} = 5.0$ was applied. Every grid cell with

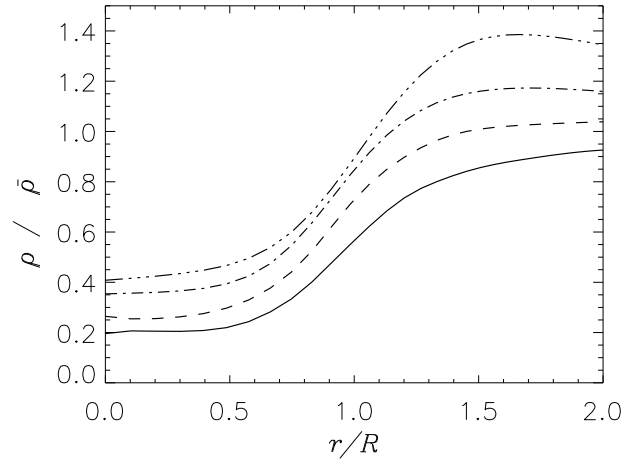
Table 3. The scaling relation in 3D for the lower quartiles, medians and upper quartiles of void size distributions in randomly diluted OCDM and FOF-halo samples and in halo samples with increasing mass.

samples	lower quartile	median	upper quartile
OCDM mocks, randomly diluted	$3.3 \pm 0.2 + (1.5 \pm 0.02) \times \lambda$	$5.2 \pm 0.1 + (2.5 \pm 0.01) \times \lambda$	$9.8 \pm 0.5 + (2.9 \pm 0.06) \times \lambda$
Λ CDM halos, randomly diluted	$3.7 \pm 0.2 + (1.5 \pm 0.02) \times \lambda$	$7.7 \pm 0.4 + (2.4 \pm 0.04) \times \lambda$	$13.5 \pm 0.8 + (3.0 \pm 0.07) \times \lambda$
Λ CDM halos, increasing mass	$1.5 \pm 0.3 + (1.8 \pm 0.02) \times \lambda$	$4.1 \pm 1.5 + (2.9 \pm 0.13) \times \lambda$	$6.2 \pm 0.8 + (4.1 \pm 0.07) \times \lambda$

**Figure 6.** The median, upper and lower quartile values of the void size distributions of DM halos with growing mass as described in Fig. 5 (squares and dotted lines), compared to diluted samples using the lowest mass threshold (diamonds and solid lines).

a density below this value was regarded as containing no significant structure. After finding the voids their density profiles were computed by averaging in concentric spheres around the center of the base voids. The density profiles as shown in Fig. 7 were obtained by averaging in size ranges between $(36 - 50)h^{-1}\text{Mpc}$, $(24 - 36)h^{-1}\text{Mpc}$, $(16 - 24)h^{-1}\text{Mpc}$ and $(10 - 16)h^{-1}\text{Mpc}$. To obtain the average between voids of different sizes we use a relative radial coordinate r/R , where r is the distance from the void center and R is the corresponding effective void radius defined above. For the study of the environment of the voids we extend the averaging to relative radial coordinates larger than unity. They are calculated up to a sphere with $r = 2R$, the last sphere contains a volume eight times larger than the void.

Two effects are obvious in the profiles shown in Fig. 7. The average underdensity at the center of voids depends on the void size. On average the central density of small voids is higher than that of large voids. This correlation reflects the inversion of gravitational clustering. While high peaks in the density fluctuations evolve to the knots in the large scale structure, large voids are formed in regions with a primordial large scale underdensity. Also the profiles show the tendency that the environment of large voids is underdense, while small voids will form both in underdense and over-

**Figure 7.** Averaged density profiles of under dense regions in a Λ CDM2 simulation with $200h^{-1}\text{Mpc}$ box size. The average is taken in size ranges $36h^{-1}\text{Mpc} - 50h^{-1}\text{Mpc}$ (solid line), $24h^{-1}\text{Mpc} - 36h^{-1}\text{Mpc}$ (dashed line), $16h^{-1}\text{Mpc} - 24h^{-1}\text{Mpc}$ (dashed-dotted line) and $10h^{-1}\text{Mpc} - 16h^{-1}\text{Mpc}$ (dashed-3dotted line).

dense regions. This is typical for the hierarchical clustering scenario.

6 EVOLUTION OF VOIDS

A study of the void evolution using an adhesion model of structure formation was carried by Sahni et al. (1994). There a correlation of the void size with the value of the primordial gravitational potential was suggested, and it was derived a redshift dependence of void sizes, $D(z) = D_0/(1+z)^{1/2}$. More recently, Friedmann and Piran (2000) proposed a model that combines the growth rate of negative density perturbations with a lower probability of galaxy formation in these underdense regions. According to this model a typical void with a size of $20h^{-1}\text{Mpc}$ corresponds to a 3σ perturbation so that they occur very rarely. This simple model can explain relatively large voids in the case of a Λ CDM universe, but it still fails to reproduce the occurrence of as large voids as observed in the LCRS (Müller et al. 2000), or in the ORS and IRAS Galaxy catalogues, (El-Ad & Piran 2000).

Here we make use of the Λ CDM3 simulation in a $200h^{-1}\text{Mpc}$ box. In addition to the resulting dark matter distribution at present epoch, we stored the snapshots of

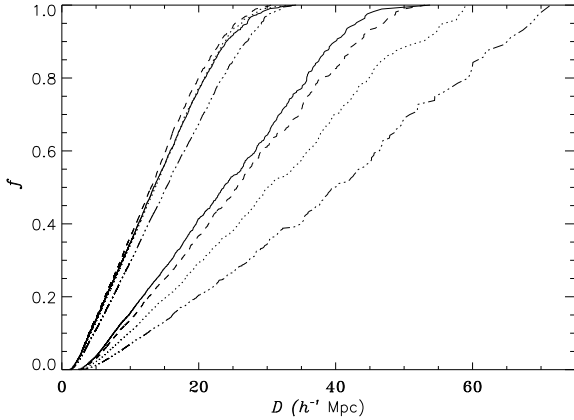


Figure 8. Cumulative size distribution of voids among dark matter halos in a Λ CDM simulation with $200h^{-1}\text{Mpc}$ size. The solid lines refer to $z=0$, dashed, dotted and dashed-dotted lines refer to $z=1$, $z=2$, and $z=3$, respectively. The distributions to the left are obtained in the case of complete halo distributions, and the others belong to the case with a lower cutoff in the circular velocity $v_{\text{circ}} = 200 \text{ km/s}$.

the evolution at $z = 1$, $z = 2$ and $z = 3$. With the FOF-algorithm described above, gravitationally bound dark matter halos were identified at each time step to study the effects of void size evolution. A minimum of 8 dark matter particles was chosen as a requirement for the halo identification, but we keep in mind that these low mass halos are not well resolved and quite unstable to disruption in the tidal fields of neighboring halos. These halos have a minimum mass of $3 \times 10^{11} M_{\odot}$. Furthermore we constructed halo samples with a minimum circular velocity $v_{\text{circ}} = \sqrt{GM/r_{\text{vir}}} = 200 \text{ km/s}$ within the virial radius r_{vir} .

As Fig. 8 shows there is little sign of evolution up to a redshift of $z = 2$ if we consider the complete samples. This means that void sizes grow in the same rate as the Hubble expansion. The network of high and low density regions in the universe has been formed in an early epoch of the cosmic evolution. But on the other hand a significant evolution of the void distribution is observed when we consider halos larger than a certain mass or circular velocity. This implies that after the early setup of the large scale network the matter flows along the walls and filaments, continues to merge and forms larger objects with time. At the redshift $z = 1$, the evolution of the number density is already visible in the void distribution. At redshifts higher than unity, large halos are still in the stage of forming. Their number density is significantly lower, and the voids in the spatial halo distribution are increasing in comoving coordinates. The formation of more massive objects leads to a subdivision of voids as we approach redshift $z = 0$.

The evolution of the underdense regions is accompanied by a flow of dark matter from low dense to high dense regions. Here we study the evolution of the density profiles as described above. The resulting averaged density profiles are shown in Fig. 9 at different redshifts. The density profiles develop distinctly for different sizes. The value of the average

density in the central parts decreases linearly in all panels with $\delta = 0.18$ per redshift unit. The upper left panel of Fig. 9 corresponds to the largest underdense regions. Different from the other size ranges, the average density in the environment of such voids decreases during the evolution from $z = 3$ to $z = 0$.

In the upper right and lower left panel of Fig. 9, which show the profiles of median size underdense regions, the average density of the void environment remains nearly constant and roughly at mean cosmic density. In the lower right panel, which corresponds to smaller voids, the average density in the environment grows with redshift. Fig. 9 illustrates the flow of dark matter from low into high density regions mainly surrounding the small voids. A correlation between regions with positive initial gravitational potential and underdense regions was also found in (Madsen et al. 1998), in good agreement with our interpretation. There it was also found a decreasing average density in the underdense regions.

7 DISCUSSION

The present paper includes an extension of our previous analysis of the void size distribution in the 2D samples of the LCRS. By comparison of large 3D boxes with mock 2D slices in similar geometry as the LCRS we can extend our previous results. Although there is more scatter and uncertainty in the statistical measures of the void sizes in 2D, there is evidence that these results are physically relevant for the complete spatial distribution of galaxies. From the simulations we find a strong hint that the observed scaling relation of effective void sizes with the mean galaxy separation in the LCRS samples has a counterpart in the 3D structure. The effective size was defined both in 2D and 3D as the diameter of the equal sized circle or sphere as the voids. The two differ only by a nearly constant offset, i.e. the 3D void sizes that occupy the same volume fraction (or area for 2D) are about 20% smaller. We test the robustness of the scaling relations of the LCRS by evaluating the variances that the differently selected homogeneous samples, the differently oriented grids, and the dilutions introduce into the results. Other possible sources of systematic errors, such as the influence of the selection function and geometry and boundary effects, were investigated by our previous paper. The uncertainty due to these effects was found to be less than 10%.

The next part of our analysis is devoted to the question of how the void sizes in the spatial distribution of some objects depend on the type of objects. Here we study the dependence for halos of milky way mass and above. Below this mass range there might be some inconsistency of the galaxy population in voids between the observational data and models of galaxy formation (Peebles 2001). As we restrict our samples to higher mass halos, it is naturally to expect that the identified voids are larger, just because the number density of halos decreases and the mean halo separation becomes larger. An important result obtained with our analysis is that larger voids sizes are found for halos with larger mass. This effect is shown by comparing the scaling relation for samples with increasing halo masses and diluted

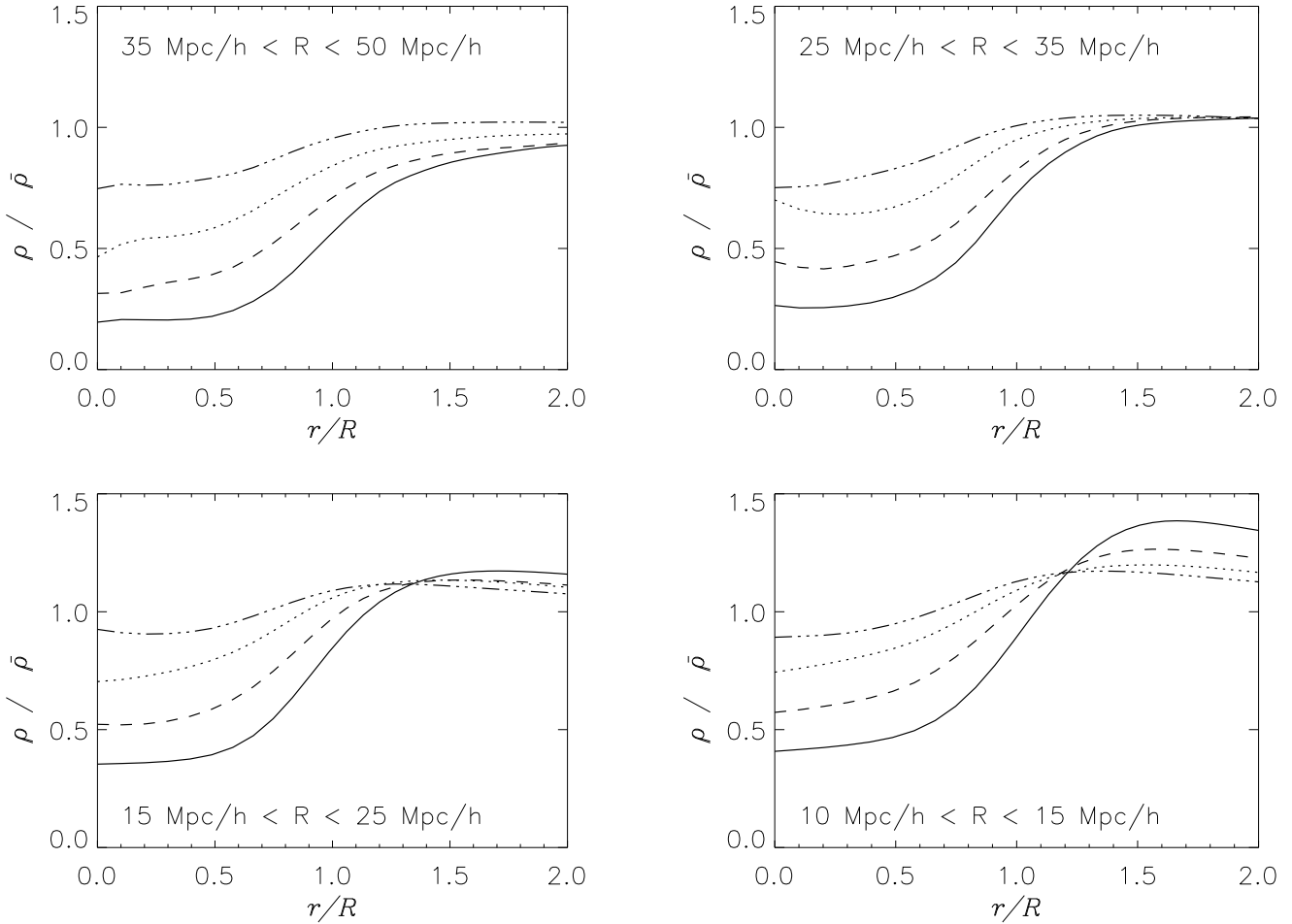


Figure 9. The evolution of average density profiles for voids in the same ranges as in Figure 7. Each panel shows the evolution in one size range, from top left the largest voids to lower right the smallest ones. The profile curves in each panel correspond to different epochs, $z=0$ (solid lines), $z=1$ (dashed lines), $z=2$ (dotted lines) and $z=3$ (dashed-3dotted lines) and illustrate the evolution in each size range.

subsamples of the original sample with equal mean density. In the latter case the voids are smaller and the slope of the scaling relation is shallower because a mixture of halos with different masses is less clustered than the comparable sample of only high mass halos. Also in this respect the scaling relation of void sizes proves to be a good measure for the fundamental clustering properties of a sample. Our new statistics extends the void probability function that was shown to provide a generating function for the set of higher order correlation functions (White 1979, Sheth 1996). It is more sensitive to the large scales in the cosmic network of galaxy structures.

Furthermore we discussed the void density profiles. These were estimated by averaging in spherical shells around the void centers. They show characteristics which are typically different for large and small voids. The central and environmental density of large voids are significantly lower than small voids. The underdensity around a large void encompasses a larger volume than the void itself, while the environment of small voids represents in the average an over-

dense ridge. We also examined the evolution of void profiles up to a redshift $z = 3$. The central underdensity decreases linearly with $\delta = 0.18$ per redshift unit. Also the environmental underdensity of large voids becomes deeper during the evolution. For average sized voids the environment density remains constant near the mean matter density, while the overdensity ridge of small voids grows. Regarding the size distribution and volume fraction of voids we find little sign of evolution in catalogues containing small dark matter halos. However if we restrict the samples to larger mass halos comparable to the milky way, there is a significant evolution in their number density and consequently in the void distribution. As they continue forming they subdivide existing voids and shift the void size distribution towards lower sizes in comoving coordinates.

The exploration of the void size evolution and of the void scaling relation in new redshift catalogues and in more realistic model galaxy distributions than considered here represents a challenging prospect for the future. It should allow a quantitative understanding of the large scale envi-

ronmental dependence of galaxy formation and its bias that should be basic for resolving the discrepancy of the scaling relation of the void size distribution function in the LCRS and in CDM models. In this way we can find an answer to the question, whether this discrepancy is a fundamental problem for the standard Λ CDM model or whether it can be explained by a more realistic description of the galaxy formation than it was possible by a nonlinear bias and by our friend-of-friends halo finder.

ACKNOWLEDGEMENTS

Sincere gratitude is due to the anonymous referee for useful and detailed comments. S.A.B. acknowledges support from the German Science foundation (DFG - Mu 6/1). We employed the AP3M code for the simulations kindly made public by H. Couchman.

REFERENCES

- Aikio J., Mähönen P., 1998, ApJ 497, 534
 Borgani S., Rosati P., Tozzi P., Stanford S.A., Eisenhardt P.E., Lidman C., Holden B., Della Ceca R., Norman C., Squires G., 2001, ApJ 561, 13
 Cole S., Hatton S., Weinberg D.H., Frenk C.S., 1998, MNRAS 300, 945
 Couchman H.M.P., 1991, ApJ 368, L23
 Doroshkevich A.G., Müller V., Retzlaff J., Turchaninov V. 1999, MNRAS 306, 575
 Einasto J., Corwin H.G., Jr., Huchra J., Miller R. H., Tarenghi M., 1983, in West R.M., ed., Highlights of Astronomy Vol. 6, Proc. 18th General Assembly of the IAU. Reidel, Dordrecht, p. 757
 Einasto J., Einasto M., Gramann M. 1989, MNRAS 238, 155
 El-Ad H., Piran T., 2000, MNRAS 313, 553
 Friedmann Y., Piran T. 2001, ApJ 548, 1
 Goldhaber G., Groom D., Kim A. et al., 2001, ApJ 558, 359
 Jaffe A., Ade P., Balbi A., et al., 2001, Phys. Rev. Lett. 86, 3475
 Kates R., Müller V., Gottlöber S., Mucket J., Retzlaff J, 1995, MNRAS 277, 1254
 Hoyle F., Vogeley M.S., 2001a, ApJ submitted, astro-ph/0109357
 Hoyle F., Vogeley M.S., 2001b, in Treyer M., Tresse L., eds, Where is the matter?, astro-ph/0110449
 Kauffmann G., Fairall A.P., 1991, MNRAS 248, 313
 Little B., Weinberg D H., 1994, MNRAS 267, 605
 Madsen S., Doroshkevich A.G., Gottlöber S., Müller V., 1998, A&A 329, 1
 Müller V., Arbabi-Bidgoli S., Einasto J., Tucker D., 2000, MNRAS 318, 280
 Oort, J. 1983, in Abell G.O., Chincarini G., eds, Early evolution of the universe and its present structure, Proc. IAU-Symp. 104. Reidel, Dordrecht, p. 1
 Peebles P.J.E., 2001, preprint astro-ph/0101127
 Plionis M., Basilakos S., 2001, MN in press, preprint astro-ph/0106491
 Sahni V., Sathyaprakash B.S., Shandarin S.F., 1994, ApJ 431, 20
 Sheth R., 1996, MNRAS 278, 101
 Tucker D.T., Oemler A., Kirshner R.P., Lin H., Shectman S.A., Landy S.D., Schechter P.L., Müller V., Gottlöber S., Einasto J., 1997, MNRAS 285, L5
 van de Weygaert R., van Kampen E., 1993, MNRAS 263, 481
 White S., 1979, MNRAS 186, 145